Rotational state populations in $^{16}O + ^{154}Sm$ near-barrier fusion

J. D. Bierman, A. W. Charlop, D. J. Prindle, R. Vandenbosch, and D. Ye
Nuclear Physics Laboratory, University of Washington, Seattle, Washington 98195
(Received 19 March 1993)

The ground state rotational band populations for the $4n$ evaporation channel have been measured at three ^{16}O bombarding energies. The populations for the $^{4}He + ^{166}Er$ reaction, which populates the same residual nucleus at above-barrier energies, have also been measured to calibrate the statistical model which has been used to relate the observed populations to the compound nuclear spin distribution. The mean compound nuclear angular momenta are somewhat less than obtained in a previous gamma ray multiplicity investigation and are in better agreement with coupled channels calculations.
PACS number(s): 25.70.Jj

I. INTRODUCTION

Heavy ion induced fusion reactions are known to be considerably enhanced over expectations for penetration of one-dimensional Coulomb plus centrifugal plus nuclear potential barriers. This enhancement is generally understood in terms of coupling to other degrees of freedom such as nucleon transfer and collective rotations and vibrations. The relative importance of these degrees of freedom as well as the contributions of more complicated rearrangements such as neck formation is still a matter of some debate.

The total fusion cross section can be thought of as the zeroth moment of the partial wave distribution leading to fusion. Additional information is contained in the higher moments of the angular momentum distribution. A number of experimental probes have been exploited to study angular momentum distributions. These include gamma ray multiplicity [1–3], fission fragment anisotropy [4–6], and isomer ratio measurements [7, 8]. These and other methods and results obtained by them have been discussed in a recent review article [9]. Although for a fair number of reactions the results are in reasonable agreement with expectations, there are a considerable number of results that show an unexpectedly large mean angular momentum very near to the barrier. The $^{16}O + ^{154}Sm$ reaction is one of the systems where gamma ray multiplicity measurements indicate a larger than expected mean angular momentum [2, 10]. We have therefore decided to reinvestigate this reaction using a different experimental probe.

The method employed here is to use the intensities of gamma transition deexciting levels in the ground state rotational band following a (HI,xn), where HI is heavy ion, reaction to determine the feeding pattern of the levels. The E vs J diagram shown in Fig. 1 illustrates the method. Since the neutrons and prerotational band statistical gammas carry off little angular momentum, maybe $2\hbar$ for four neutrons and $(1–2)\hbar$ for the statistical gammas, the population entering the ground state band at each level should be related to the initial spin distribution of the compound nucleus. For example, the difference in the intensity of the $6\rightarrow4$ transition and the $8\rightarrow6$ transition is the entrance intensity of the 8^+ ground state which should give us an idea of the population of the compound nucleus around $10\hbar$ which is entering the $4n$ channel. So, taking these differences over the entire rotational band spectrum would also give us an idea of the shape of the spin distribution of the compound nucleus which ends up in the $4n$ channel. Due to fraction-

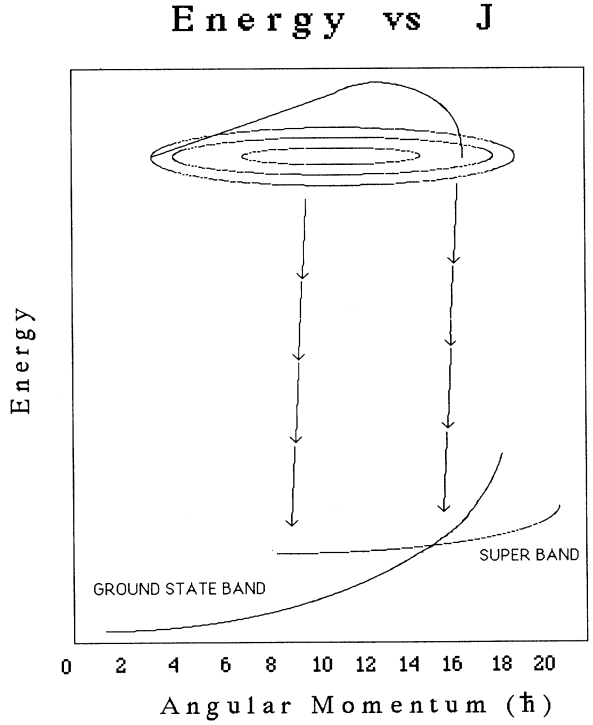

FIG. 1. The contour lines indicate schematically the compound nuclear spin distribution, whose distribution in J is shown by the topmost curve. The energy and angular momentum carried off by each neutron are indicated by the arrows. Several "statistical" gammas (not shown) typically connect the levels populated by neutron evaporation and the rotational band.

ation and other factors the distribution entering the $4n$ channel is not the same as that of the compound nucleus but can be related to it by statistical model calculations. This method is similar to an isomer ratio study except it is much more differential since many spin states can be studied rather than just two.

A previous measurement of rotational state populations had been performed for the $^{16}O + ^{154}Sm$ reaction [10] using only an unsupressed GeLi detector but the results were limited due to the Compton background of higher-energy gamma transitions obscuring peaks and causing greater uncertainty in the gamma intensity measurements. The present study has much improved sensitivity due to the use of Compton-suppressed Ge detectors and coincidence techniques. The necessary statistical model calculations to relate final rotational band feeding intensities to the compound nuclear spin distribution have been calibrated using an above-barrier reaction which makes the same compound nucleus [2].

II. EXPERIMENTAL METHOD

The systems for which we have studied the experimental rotational band spectra are $^{16}O + ^{154}Sm \longrightarrow ^{170}Yb$ and $^{4}He + ^{166}Er \longrightarrow ^{170}Yb$. The oxygen system was studied at 63, 65, and 68 MeV laboratory bombarding energies. The alpha system was studied at 43 and 47.6 MeV laboratory bombarding energies. The alpha energies were chosen to match excitation energies with the upper and lower oxygen energies. The ^{16}O beam was provided by the University of Washington FN tandem and the ^{4}He beam was obtained using the tandem in conjunction with the superconducting linac booster.

A. Setup

The experimental setup consisted of three detectors. First, a GeLi detector was placed at $-90°$ to the beam at 4 cm from the target. In addition, we used two Compton-suppressed intrinsic germanium detectors. Both of these detectors were positioned 16.5 cm from the target, one at 90° to the beam and the second at 125°. For the 63 and 65 MeV oxygen and the 43 MeV alpha runs a third intrinsic germanium detector was added. For this setup GeLi was again at $-90°$ and the intrinsic germanium detectors were at 45°, 90°, and 135°. Low-energy gammas of no interest were attenuated by placing 0.19 cm Cu absorbers in front of each Ge detector. Energy calibrations and efficiencies for the detectors were obtained by placing calibrated sources at the target position.

B. Targets

The Sm target was a self-supporting ^{154}Sm 98.7% enriched foil of 450 μg cm^2 thick. The purity of the target is important to minimize high-energy gammas from low Z contaminants. This target was produced at Oak Ridge National Laboratory. The ^{166}Er target was 325 $\mu g/cm^2$ thick.

C. Detectors

The 50 cm^3 GeLi detector is used to gate on the lower energy 200 keV–550 keV transitions in the rotational band. A GeLi detector was chosen for this purpose because its efficiency drops off quickly for higher-energy gammas which are of no interest to us. This helps keep the counting rate down in GeLi. The actual efficiency of the GeLi detector in the region of interest is not important to us, only that it drops off for higher-energy gammas.

The 236 cm^3 intrinsic Ge detectors have resolutions of approximately 2 keV at 1.33 MeV and 800 eV at 133 keV using a 6 μs shaping time. Without the Compton suppression the photopeak accounts for 36% of the area under the curve for the spectrum of a ^{137}Cs source. With the Compton suppression the photopeak accounts for 73% of the area for the same source. The Compton suppression is achieved by use of a bismuth germanate (BGO) detector designed such that there is a well in which the Ge detector is placed from above and has a window which opens towards the target. The front face of the BGO detector is shielded from the target area by a 2.5 cm thick tungsten shield with a matching window.

III. ANALYSIS

The data are analyzed off line. First, gates are set in the time difference spectra between the GeLi and each Ge detector. Then, for any event occurring within the prompt peak gate in the time difference spectra, the energy spectra for the GeLi detector is incremented in the appropriate data area; one data area for coincidences with $G1$, one for coincidences with $G2$, and another for coincidences with $G3$ (for the later runs). We are then able to set a gate in the GeLi energy spectra on whichever peak we wish to gate on to further "clean up" the energy spectra in the germanium detectors. We can also look at the coincidences between the germanium detectors in the same way treating one as a "GeLi" for gating puposes and then looking at the cleaner spectra in the other germanium detector. The $2\rightarrow0$ transition is highly converted so the lowest transition we can detect is the $4\rightarrow2$ transition. We then resort the data only updating the Ge detectors energy spectra if the GeLi event is within our gate on that energy spectra. The data are then sorted again with the gate in the GeLi spectra shifted off of the peak for purposes of background subtraction. The difference between these spectra is then our raw rotational band spectra gated on the $4\rightarrow2$ transition in another detector. We then combine the three spectra correlating to energy gates in the three other detectors to give us the energy spectra of either of the Ge detectors gated on the $4\rightarrow2$ transition in the other detectors. Figure 2 shows a sample spectrum of one of the Ge detectors gated on the $4\rightarrow2$ transition in the other detectors.

This process is repeated gating on the $6\rightarrow4$, $8\rightarrow6$, and $12\rightarrow10$ transitions. We found that the $10\rightarrow8$ transition's energy, 507.4 keV, was too close to other transition energies, particularly $18_s \rightarrow16_s$ at 509 keV, to be distinguished for reliable gating purposes. The subscript s is

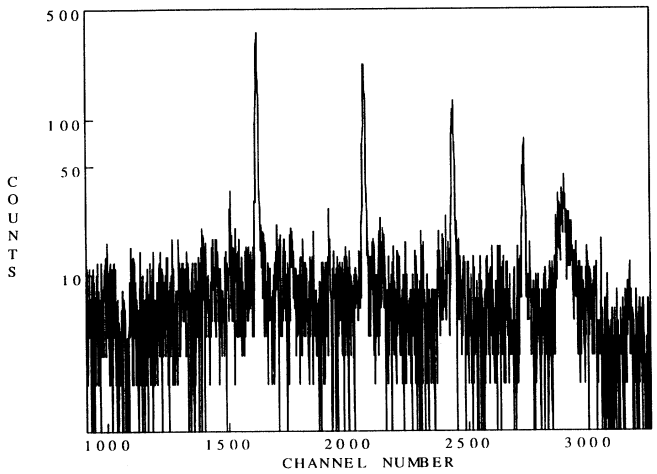

FIG. 2. Sample spectrum of a Ge detector gated on the 4→2 transition in the energy spectra of the other detectors.

used to denote states which are not in the ground state rotational band but are in a "superband" or largely deformed band in the ^{166}Yb nucleus [11]. This superband causes some minor problems in the evaporation model calculations which will be discussed later. The important point here though is that if two peaks are used simultaneously for gating purposes then the intensity ratios can be affected thus compromising our results.

Once we have the gated energy spectra, the areas for the peaks correlating to transitions occurring higher in the rotational band than the transition used as a gate are extracted. These areas are corrected for detector efficiency and internal conversion. Now, we are interested in finding the ratio of the intensities of adjacent transitions. We also want to use as many sorts as possible for each ratio. So, the 8→6 / 6 →4 ratio is determined from the data sort which was gated on the 4→2 transition. The 10→8 / 8→6 ratio is found by averaging over both the sort gated on the 4→2 transition and the sort gated on the 6→4 transition. The 12 →10 / 10→8 and the 14→12 / 12→10 ratios are determined by averaging over those two sorts plus the sort gated on the 8 →6 transition. The $16_s \rightarrow 14$ / 14 → 12 ratio is taken from the sort gated on the 12 →10 peak because it yields the cleanest $16_s \rightarrow 14$ and 14→12 peaks. Finally, the 6→4 / 4→2 ratio is taken from singles data. We obtained values for the 6 →4 / 4→2 ratio up to the $16_s \rightarrow 14$ / 14→ 12 ratio for the alpha system at both energies and the oxygen system at both 68 MeV and 65 MeV. We were unable to determine the last two ratios for the oxygen system at 63 MeV due to the weak intensity of the last two transitions.

IV. EVAPORATION MODEL PARAMETRIZATION

The ^{4}He + ^{166}Er data were used to calibrate the gamma decay strength parameters in the evaporation model code PACE [12] as modified by Beene [13] to employ a giant dipole resonance form for the $E1$ gamma strength function. We take the relative xn yields for the ^{4}He + ^{166}Er system and the total cross section from a previous work as fixed parameters for the calculation. We can safely predict what the spin distribution should be for this very asymmetric system at energies well above the barrier. Using the three constraints of the total fusion cross section, relative xn yields, and the calculated compound nucleus spin distribution, the decay parameters $E1$, $M1$, $E2$, $M2$, $\beta(2)$, and the stretched collective (SC) strength are adjusted so that PACE will yield the determined experimental transition intensity ratios. The parameters $M1$, $E2$, and $M2$ are gamma transition strengths in Weisskopf units for $M1$, $E2$, and $M2$ transitions respectively. An $E1$ strength function is used and the classical Lorentz shape is employed. The $E1$ parameter becomes the fraction of the energy weighted sum rule exhausted by the integrated $E1$ strength. A split giant dipole resonance is used, with the splitting determined by the deformation parameter $\beta(2)$. The parameter SC is the strength, in Weisskopf units, of the collective $E2$ transitions. The corresponding width is added to the width obtained from the $E2$ parameter if ΔJ is 2 and the transition energy, modulo the energy binning, is equal to the stretched $E2$ transition energy expected from the yrast line used in the calculation. The parameters were first determined with the 48 MeV data and then checked with the 43 MeV data. The rotational state population intensity comparisons are shown in Table I.

The only problem appears with the last two ratios. This problem is caused by the superband in the ^{166}Yb level diagram. This superband crosses the 0^+ ground state band between levels 14 and 16 [11]. The evaporation model code is not sophisticated enough to understand this crossover point which is not unexpected. Whereas experimentally we find the population almost totally in the 14^+ ground state, the code places a comparable amount of the population in the 14^+ superband state. This is observed by the presence of a $14_s \rightarrow 12_{gr}$ transition in the PACE results and its absence in the experimental results. If this population had gone to the 14_{gr} state then the 14→12 transition would be of higher intensity. This would decrease the 16 →14 / 14→12 ratio and increase the 14→12 / 12→10 ratio which explains the effect we see in the results table. The values for the gamma decay strength parameters which reproduced the experimental transition intensities were $E1 = 1.9$, $M1 = 0.025$, $E2 = 120$, $M2 = 2.5$, SC = 120, and $\beta(2) = 0.3$. It was a nontrivial exercise to find a set of these parameters which were not unphysical and that reproduced the experimental results. We found that the intensities appeared to be most sensitive to changes in the $E2$ strength and the deformation parameter $\beta(2)$ value.

Now that the decay parameters for the evaporation code PACE are determined we are ready to look at the oxygen system. Since we have experimentally determined the transition intensities and we have the decay parameters fixed for the ^{170}Yb compound nucleus, the only thing left which can vary is the shape of the spin distribution of the compound nucleus. The total area is determined by the known cross section [14]. The shape is assumed to be of the form of $1/(1+e^{(l-40)/\text{diffuseness}})$ and we vary

TABLE I. Experimental and calculated ratios of consecutive rotational band transitions for the ^{4}He + ^{166}Er reaction at both 43 and 47.6 MeV laboratory bombarding energies.

Transition	48 MeV expt.	48 MeV PACE	43 MeV expt.	43 MeV PACE
4→2				
	0.876 ± 0.066	0.887 ± 0.018	0.847 ± 0.076	0.826 ± 0.017
6→4				
	0.766 ± 0.057	0.807 ± 0.018	0.680 ± 0.022	0.766 ± 0.017
8→6				
	0.752 ± 0.061	0.746 ± 0.019	0.665 ± 0.023	0.652 ± 0.018
10→8				
	0.591 ± 0.046	0.587 ± 0.018	0.534 ± 0.016	0.526 ± 0.019
12→10				
	0.621 ± 0.042	0.435 ± 0.019	0.497 ± 0.018	0.362 ± 0.020
14→12				
	0.329 ± 0.035	0.403 ± 0.028	0.299 ± 0.027	0.351 ± 0.033
16→14				

the diffuseness parameter. We vary this last parameter of the code until the PACE transition intensities match the experimental transition intensities for each of the three energies for the oxygen system. We can then compare $\langle \ell \rangle$ from this distribution with the $\langle \ell \rangle$ results from other experiments. In addition to just the average spin, we also have information on what the actual distribution looks like, as will be discussed later. The experimental rotational state intensity results as well as the matching PACE results are listed in Table II.

Other than the same effect in the last two ratios that we observed in the alpha system, we have a relatively good match in ratios. The only parameter which is varied from energy to energy, other than using the correct total cross section and relative xn yields, is the spin distribution of the compound nucleus, ^{170}Yb. Another helpful plot to see the overall fit of the transition intensities is to plot the intensity vs $j(j+1)$ for both the experimental results and the PACE results normalized to the 4→2 transition. This gives a better overall feel for how well the PACE results fit the experimental values. Plots for all five sets of data are shown in Fig. 3.

Other than the discussed discrepancy at the band crossover point, we get very reasonable matches to the experimental results. We would now like to see how our values for the average spin of the compound nucleus compare with those measured in previous experiments. For this purpose we have plotted, in Fig. 4, our values for the ^{16}O + ^{154}Sm system at the three laboratory energies we used along with the results from previous discrete gamma-tagged multiplicity experiments and evaporation residue-tagged multiplicity experiments. Our values are the average spins of the compound nucleus distribution found in the evaporation code calculation which best fit the experimental rotational band intensities. The full curve is from a coupled channels calculation using the code CCDEF [15]. For this calculation ^{154}Sm was assumed to have static quadrapole and hexadecapole deformations with $\beta 2 = 0.29$ and $\beta 4 = 0.07$.

Observe that our results agree quite well with the coupled channels calculation and are slightly lower than the previous experimental results.

We should also look at the spin distributions of the compound nucleus in the two systems. For the alpha

TABLE II. Experimental and calculated ratios of consecutive rotational band transitions for the ^{16}O + ^{154}Sm reaction at 63, 65, and 68 MeV laboratory bombarding energies.

Transition	68 MeV expt.	68 MeV PACE	65 MeV expt.	65 MeV PACE	63 MeV expt.	63 MeV PACE
4→2						
	0.835 ± 0.066	0.830 ± 0.010	0.681 ± 0.060	0.739 ± 0.010	0.677 ± 0.041	0.650 ± 0.013
6→4						
	0.672 ± 0.044	0.753 ± 0.010	0.644 ± 0.038	0.648 ± 0.010	0.554 ± 0.029	0.596 ± 0.015
8→6						
	0.737 ± 0.052	0.677 ± 0.011	0.625 ± 0.037	0.571 ± 0.012	0.517 ± 0.028	0.490 ± 0.017
10→8						
	0.555 ± .041	0.548 ± 0.012	0.512 ± 0.029	0.488 ± 0.014	0.469 ± 0.029	0.448 ± 0.023
12→10						
	0.660 ± 0.059	0.435 ± 0.013	0.574 ± 0.039	0.371 ± 0.017		
14→12						
	0.360 ± 0.051	0.444 ± 0.021	0.273 ± 0.030	0.360 ± 0.027		
16→14						

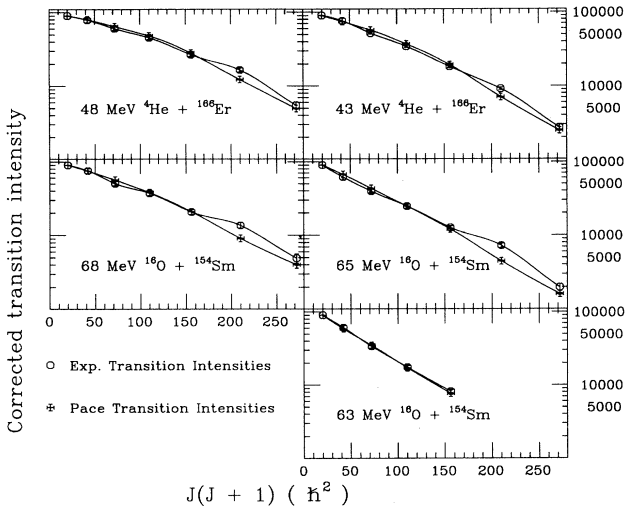

FIG. 3. Rotational band transition intensities from both experiment and evaporation model code.

system, as mentioned before, for an asymmetric system well above the barrier we know we should have a nearly triangular distribution along the lines of a sharp cutoff model. Figure 5 shows the distributions used in doing the calibration of the decay parameters for the evaporation code.

Figure 6 shows the spin distributions which we found to reproduce the experimental rotational band transition intensities in the oxygen system at the three bombarding energies we used. As can be seen, we find that to reproduce the experimental results a very broad distribution which extends up to relatively high spins must be used in contrast to the alpha-induced reactions' relatively sharp cutoff distribution. At higher energies the distribution extends up to higher spins which accounts for the greater intensity in the transitions farther up in the rotational band.

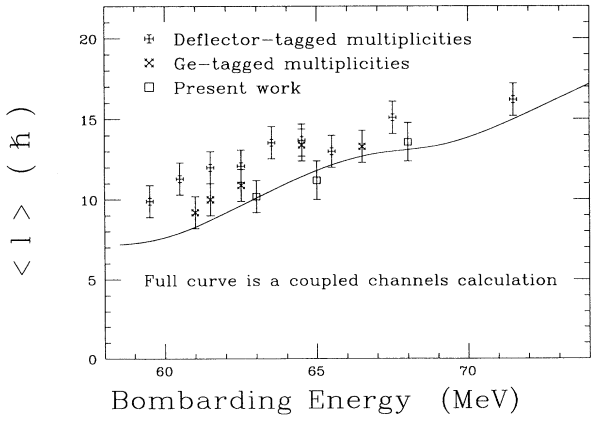

FIG. 4. Mean ℓ for $^{16}O + ^{154}Sm$ determined from conversion of the rotational band intensity ratios using the evaporation model code PACE as well as from gamma ray multiplicities determined by discrete gamma ray and deflector tagging techniques. The full curve is from a coupled channels calculation.

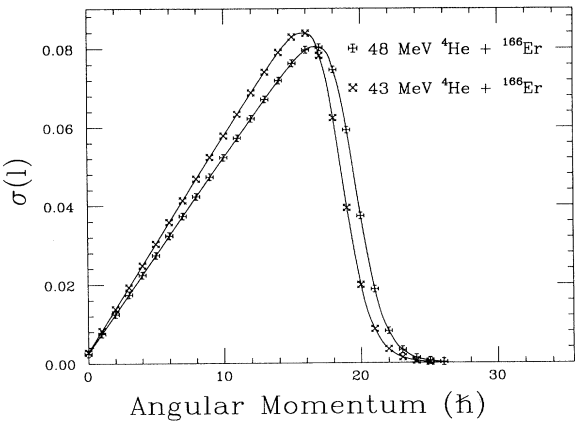

FIG. 5. Compound nucleus spin distributions of ^{4}He + ^{166}Er fusion used for the evaporation model code PACE decay parameter calibration.

Finally, we can take differences in the intensities of adjacent transitions to the ground state band to obtain information about the feeding of the $4n$ channel. Since the neutrons and statistical gamma rays carry off little angular momentum, the entrance spin distribution of the ^{166}Yb ground state band will be related to, but shifted slightly down from, the part of the compound nucleus distribution which went to the $4n$ channel. One obvious problem with this method is that we are taking differences of large numbers which are relatively close together in magnitude so having the uncertainties in the rotational state transition intensities rather low is of crucial importance for us. Statistical fluctuations can lead to distracting structure in the curves. To reduce such structure we have averaged over all adjacent pairs of differences. If these values are plotted along with the spin distribution which could be extracted from PACE in the same manner, we would see the same shape since we have tried to match the PACE intensities to the experimental transition intensities. If we plot these along with the initial

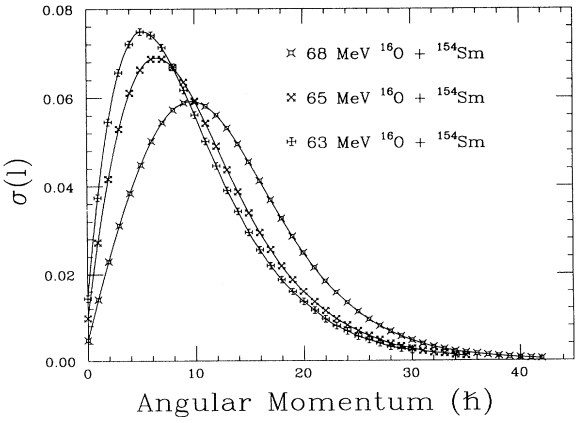

FIG. 6. Compound nucleus spin distributions of ^{16}O + ^{154}Sm fusion determined by fitting rotational band transition intensities using the evaporation model code PACE.

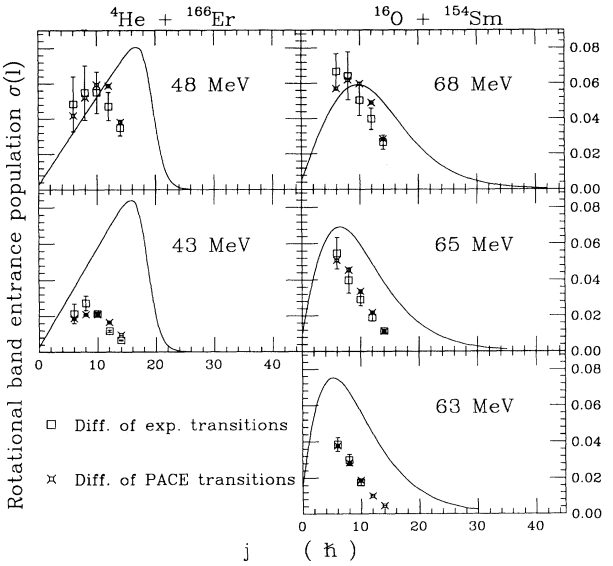

FIG. 7. Rotational band entrance populations from smoothed differences of consecutive experimental rotational state band transition intensities. Also shown is the compound nucleus spin distribution for each case.

compound nucleus spin distribution, we will be able to get a feeling for what part of the distribution in the compound nucleus is going to the $4n$ channel. Of course the difference distribution is actually offset from where the actual distribution would lie on the x axis (or displaced in spin) by about (2–4)$\hbar$ from the neutron evaporation and the statistical gammas. We have done this for all five sets of data and the results are shown in Fig. 7. The results are quite reasonable considering the difficulties of the difference method used. Due to shifting and redistribution, the feeding intensity can exceed the compound nucleus spin distribution. The shape of the curves from both the PACE results and the differences in rotational state populations seem to match rather well. We also see that we are getting more of the low spin population of the compound nucleus going to the $4n$ channel than high spin population. This is due to the reduced excitation energy available for neutron evaporation when the compound nucleus has high spin. The compound nucleus at high spins just does not have enough excitation energy to evaporate four neutrons before it reaches the yrast line. This may be easier to understand by looking at Fig. 1 in the Introduction. This is also the reason that early gamma multiplicity experiments mispredicted the average spin of compound nuclei when they only tagged on a certain channel. The $\langle \ell \rangle$ of the part of the compound nucleus which evaporates to the $4n$ channel is lower than the $\langle \ell \rangle$ of the entire compound nucleus distribution.

V. CONCLUSION

We have used a much improved detector system to determine the population of the ground state rotational band of the $4n$ channel decay of ^{170}Yb produced using two entrance channels, ^{16}O + ^{154}Sm and ^{4}He + ^{166}Er. The alpha system was used as a calibration tool for the statistical evaporation code PACE. The populations were determined more accurately and more completely than the previous detector system allowed as we were able to clean up the spectra enough so that three transitions which before were unobservable could be studied. These data were used to obtain values of the average angular momentum for the ^{16}O + ^{154}Sm system at three near-barrier energies. Our results compare well with a coupled channels calculation and are slightly lower than the results from previous multiplicity measurements. This suggests that the rotational state population method is a better probe of mean angular momentum values in the near-barrier energy regime than the multiplicity method because of the problems with converting multiplicities to mean angular momentum at near-barrier energies. We have also been able to determine a more detailed idea of what the actual spin distribution of the compound nucleus is. We found that the oxygen system at near-barrier energies had a much broader compound nuclear spin distribution than the sharp-cutoff-like distribution which can be predicted for the asymmetric, well-above-barrier, ^{4}He + ^{166}Er system. While this experimental method is limited in the number of systems which are practical for study, we have found that if a proper calibration system is also studied that useful information about the spin distribution of compound nuclei resulting from near-barrier fusion can be extracted.

This work was supported in part by the U.S. Department of Energy.

[1] A.H. Wuosmaa *et al.*, Phys. Lett. B **263**, 23 (1991).
[2] S. Gil, R. Vandenbosch, A. Charlop, A. Garcia, D.D. Leach, and S. Kailas, Phys. Rev. C **43**, 701 (1991).
[3] M.L. Halbert, J.R. Beene, D.C. Hensley, K. Honkanen, T.M. Semkow, V. Abenante, D.G. Sarantites, and Z. Li, Phys. Rev. C **40**, 2558 (1989).
[4] R.F. Reising, G.L. Bate, and J.R. Huizenga, Phys. Rev. **141**, 1161 (1966).
[5] J.P. Lestone, J.R. Leigh, J.O. Newton, and J.X. Wei, Nucl. Phys. **A509**, 178 (1991).
[6] B.B. Back *et al.*, in Proceedings of the 6th Winter Workshop on Nuclear Dynamics, Jackson Hole, Wyoming, Lawrence Berkeley Report No. LBL 28709, 1990.
[7] R.G. Stokstad, D.E. DiGregorio, K.T. Lesko, B.A. Harmon, E.B. Norman, J. Pouliot, and Y.D. Chan, Phys. Rev. Lett. **62**, 399 (1989).
[8] D.E. DiGregorio, K.T. Lesko, B.A. Harmon, E.B. Norman, J. Pouliot, B. Sur, Y. Chan, and R.G. Stokstad, Phys. Rev. C **42**, 2108 (1990).
[9] R. Vandenbosch, Annu. Rev. Nucl. Part. Sci. **42**, 447 (1992).
[10] R. Vandenbosch, B.B. Back, S. Gil, A. Lazzarini, and A.

Ray, Phys. Rev. C **28**, 1161 (1983).
[11] C.A. Fields, K.H. Hicks, M.A. Rumore, and R.J. Peterson, Phys. Lett. **130B**, 157 (1983).
[12] A. Gavron, Phys. Rev. C **21**, 230 (1980).
[13] J.R. Beene (private communication).
[14] R.G. Stokstad, Y. Eisen, S. Kaplanis, D. Pelte, U. Smilansky, and I. Tserruya, Phys. Rev. C **21**, 2427 (1980).
[15] J. Fernandez-Niello *et al.*, Comput. Phys. Commun. C **42**, 2108 (1990).